PHOTONICS Research

Highly reliable integrated W-band transmitter based on an on-chip dual-mode DFB laser and cascaded microring modulators

Xuying Liu,[1] Wenjia Zhang,[1,*] Yue Jiang,[1] Han Wang,[1] Dan Lu,[2] Fan Yang,[3] and Zuyuan He[1]

[1]State Key Laboratory of Advanced Optical Communication Systems and Networks, Shanghai Jiao Tong University, Shanghai 200240, China
[2]Key Laboratory of Semiconductor Material Science, Institute of Semiconductors, Chinese Academy of Sciences, Beijing 100083, China
[3]School of Electronic Science and Engineering, University of Electronic Science and Technology of China, Chengdu 610054, China
*Corresponding author: wenjia.zhang@sjtu.edu.cn

Received 27 December 2022; revised 24 April 2023; accepted 29 May 2023; posted 31 May 2023 (Doc. ID 484480); published 1 August 2023

We propose an integrated W-band transmitter enabled by an integrated dual-mode distributed feedback (DFB) laser and cascaded silicon photonic microring modulators for next-generation wireless communication. 10 Gb/s error-free intensity modulation and direct detection W-band transmission are achieved in experiments by using the dual-mode DFB laser and two free-running lasers. Moreover, we conduct an experiment of dual-carrier modulation based on cascaded microring modulators, achieving 3 dB signal-to-noise ratio improvement and better signaling integrity for wireless communication. The proposed photonic integrated W-band transmitter will be a viable solution for a high-speed and low-power wireless communication system.

https://doi.org/10.1364/PRJ.484480

1. INTRODUCTION

With the rise of automatic driving, virtual reality, ultra-high-definition video, and artificial intelligence applications, the demand for wireless communication will almost double every 18 months according to Edholm's law [1]. In 2022, the data traffic of wireless and mobile devices accounted for 71% of the total Internet traffic [2]. According to Shannon's formula, in order to overcome the bandwidth bottleneck, it is of necessity to seek higher-frequency carriers to contain larger data bandwidth. Millimeter wave (mmWave) technology located at 30–300 GHz has received extensive attention due to its more available spectrum resources [3,4]. The advanced technology of mmWave communication will improve the throughput of wireless data, which can meet future demand for high-capacity and low-latency wireless networks.

Photonic heterodyne generation of mmWave signals has become a viable and scalable solution, which can be extended to terahertz (THz) frequency [5–8]. The wireless transmitter based on photonic integration technology has the advantages of low loss, small size, and controlling flexibility [9,10]. Various functions of the photonic mmWave system have been realized based on silicon photonics including carrier generation, data modulation, multiplexing, and detection [11–13]. In 2020, silicon integrated circuits based on an on-chip electro-optical Mach–Zehnder (MZ) modulator was used for wireless transmission at the 300 GHz carrier frequency [12]. Most recently, an integrated THz transmitter based on an optical frequency comb injected distributed feedback (DFB) laser has been reported to realize the high-speed indoor communication application [14]. Moreover, an integrated high-speed photodetector (PD) was achieved to generate the reliable 300 GHz carrier [15,16].

However, the essence of photonic heterodyne generation is mapping of light wave to mmWave through frequency beating at the photodetector and thereby data modulated in the photonic domain are moved to the mmWave domain. Therefore, an integrated and combined hardware will be required of multi-wavelength lasers and wavelength selective data modulation. In this particular case, compared with the MZ modulator, the microring modulators have a much smaller size and importantly wavelength selectivity capability, which can be employed for wavelength-division multiplexing transmission both in light wave and mmWave [17]. The combination of integrated DFB lasers and silicon photonic interconnect circuits can form a hybrid and concise platform for future photonic wireless communication, especially for the intensity modulation and direct detection (IM-DD)-based interconnect architecture [18,19].

In this paper, we propose a W-band wireless transmission based on a high-power on-chip dual-mode DFB laser and high-speed microring modulator. This is the first attempt to use silicon photonic chips and laser chips based on microring modulators and other passive devices in photonic-assisted millimeter wave communication. In addition, we propose a scheme for synchronous modulation of cascaded microring modulators, which enables the transmission system to have

higher performance. The method of dual modulation based on cascaded microring modulators is more suitable for the use of a dual-mode laser and simplifies the system complexity.

The bit error rate (BER) performances of a 10 Gb/s wireless transmission system at 86 GHz by using a dual-mode DFB laser and two free-running lasers are compared, demonstrating that the dual-mode DFB laser, although having sideband interference, shows the same transmission performance as the free-running lasers. Moreover, the dual-carrier modulation scheme based on cascaded microring modulators is demonstrated to achieve 3 dB signal-to-noise ratio improvement and thereby better signaling integrity for the wireless transmission system [20]. The proposed photonic integrated W-band wireless transmitter will be a viable solution for a high-speed and low-power wireless IM-DD interconnect system.

2. FACTORS AFFECTING PHOTONIC WIRELESS TRANSMISSION SYSTEM

Currently, there are two main schemes for photonic heterodyne to generate wireless signals: single-carrier modulation and dual-carrier modulation. As analyzed in Ref. [20], we assume that the modulator is an ideal modulator and ignore the nonlinearity of the modulator. Figure 1(a) shows the transmission spectrum of the microring modulator under different reverse bias voltages. We assume that the average optical power of the modulated optical carrier is P_0 when the microring modulator operates at the optimal state of the eye diagram. The optical power of the reference optical carrier is P_1. It can be noted that P_0 and P_1 are the average power including coupling loss, chip insertion loss, and modulation loss. When the modulated optical carrier is located at the optimal operating point of the microring modulator, the power of the modulated optical signal is $s(t)$, which is shown in Fig. 1(b). Based on the above settings, the optical power of the modulated signal at other corresponding working points is $ks(t)$, with the value of k between 0 and 1. It can be obtained that the beating signal of the ideal intensity modulator is shown in the following equations:

$$E_3 = E_1 + E_2 = \sqrt{P_0 + k_0 s(t)}\exp(jw_1 t) + \sqrt{P_1 + k_1 s(t)}\exp(jw_2 t), \quad k_0, k_1 \in [0,1] \tag{1}$$

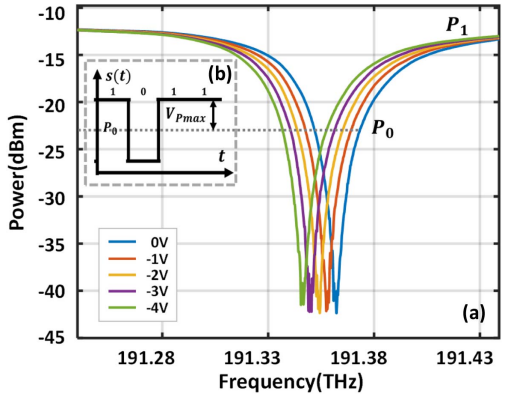

Fig. 1. (a) Transmission spectrum of the microring modulator at different voltages. (b) Modulated signal at the optimal working point.

$$I_{PD} \propto |E_3|^2, \tag{2}$$

$$|E_3|^2 = P_0 + P_1 + (k_0 + k_1)s(t) + 2\sqrt{P_0P_1 + (P_0k_1 + P_1k_0)s(t) + k_0k_1s(t)^2}\cos(w_0 t), \tag{3}$$

$$I_{ED} \propto P_0P_1 + (P_0k_1 + P_1k_0)s(t) + k_0k_1s(t)^2. \tag{4}$$

Without considering the wireless channel characteristics, there are two main factors that affect the transmission performance of the system. The first one is the average power of the wireless carrier, while the other one is the modulation depth of the signal. It can be concluded from Eq. (4) that P_0P_1 determines the power of the wireless carrier. The condition of maximum wireless carrier signal delivery is $P_0 = P_1$. Since the input optical power of the PD has an upper limit, the two modulated optical carriers with similar average power can obtain higher wireless signal when the total power is the same.

The second factor is the modulation depth of the optical signal, which is related to the value of $P_0k_1 + P_1k_0$. The value of k_0 and k_1 is related to the selected working point of the microring modulator. As is shown in Fig. 1(a), the single-carrier modulation conditions are $k_0 = 1$ and $k_1 = 0$. The modulation depth of the wireless signal is proportional to $P_0s(t)$. In order to improve the modulation depth, we can obtain the theoretical power of the carrier signal, which is proportional to the following equation under the condition of $k_0 = k_1 = 1$ in Eq. (4):

$$I_{ED} \propto P_0^2 + 2P_0s(t) + s(t)^2. \tag{5}$$

When the two optical carriers are modulated at once and both operated at the optimal operating point of the microring modulator, the modulation depth could increase by 3 dB. However, due to the narrowband transmission characteristics of the microring modulator shown in Fig. 1, only one single microring modulator cannot realize the simultaneous modulation of two optical carriers in most cases. We have to mention that the case where the frequency difference is exactly around one free spectral range (FSR) of the microring modulator has been eliminated. Therefore, in order to realize the simultaneous modulation of two carriers like MZM, two cascaded microring modulators loading the same signal are required.

3. W-BAND WIRELESS TRANSMISSION SYSTEMS

A. Experimental Setup Based on Photonic Integrated Circuit

Figure 2 shows the experimental setup for a W-band IM-DD communication system to demonstrate the integrated transmitter based on a chip-based DFB laser and photonic integrated circuit (PIC). In the current experiment, the integrated transmitter, including a III-V based laser and a silicon modulator chip, is combined by optical fibers. The total coupling loss of the chip is about 5–7 dB. The dual-mode DFB laser, shown in Fig. 2(a), follows a high-power design with four pairs of

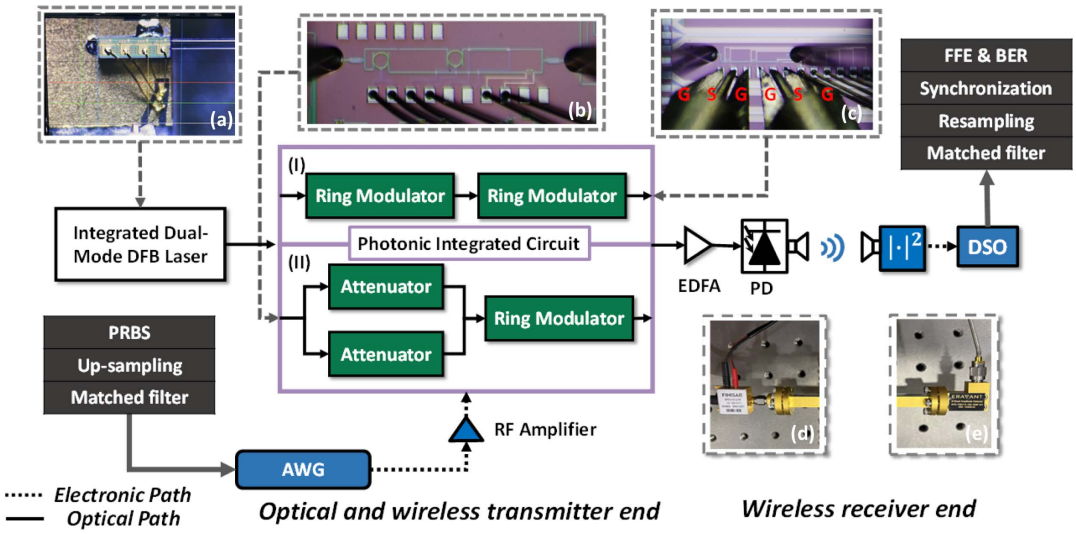

Fig. 2. Experimental setup for a W-band IM-DD wireless communication system based on the photonic integrated circuit (PIC). (a) On-chip dual-mode DFB laser. (b) PIC containing a single microring modulator and ring resonators. (c) PIC containing cascaded microring modulators. (d) High-speed photodetector with a W-band transmitting antenna. (e) Envelope detector with a W-band receiving antenna.

compressively strained AlGaInAs quantum wells and a cavity length of 1000 μm. A buried InGaAsP-based Bragg grating is used for longitudinal mode control. A double-trench ridge waveguide structure with a ridge width of 2.3 μm is used for lateral mode control. Two lasing modes can be obtained for lasers with a proper grating phase. The size of the laser chip is about 0.33 cm^2.

Figure 3(a) shows the optical spectrum of the DFB laser versus different input currents. It can be seen that the output spectrum of the DFB laser does not have dual modes under all current conditions. Therefore, it is necessary to match the best working point of the microring modulator with the wavelength of the dual-mode DFB laser. The original digital signal sequence is composed of the synchronization head, training sequence, and pseudorandom binary data sequence. The training sequence is used to train the tap coefficients for equalization.

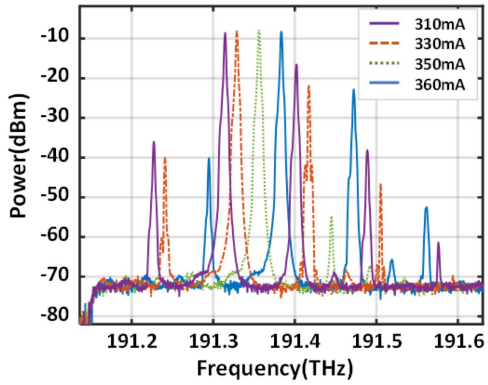

Fig. 3. Dual-mode and single-mode of integrated DFB laser at different input currents.

The electric signal generated by arbitrary waveform generator (AWG) (Keysight M8195A) is amplified after rising cosine filtering. The amplified signal is loaded to the silicon photonic chips, including one chip with a single microring modulator and wavelength filters and the other with two cascaded microring modulators. The footprints of the two kinds of silicon photonic circuits are 0.36 cm^2 and 0.28 cm^2, respectively. The various silicon photonic chips are designed for verifying the versatile functionality of the photonic domain to enable reliable W-band wireless communications. The output modulated optical signal of the PIC is converted into an electromagnetic wave for radiation driven by a high-speed photodetector with a 15 dBi antenna. At the receiving end, the received signal is downconverted to baseband through a 10 GHz video bandwidth envelope detector (SFD-753114-103-10SF-N1) with a same gain antenna. The received signal collected by an oscilloscope is processed by off-line digital signal processing including matching filtering, resampling, synchronization, and feed forward equalizer (FFE) equalization for bit error rate statistics.

B. Experiments of Single-Carrier Modulation

Since the transmission spectral line is a Lorentz curve, the wavelengths of the two optical carriers used to generate the mmWave signal are located at the optimal modulation working point of the modulator and the straight through part of the transmission spectrum. The power difference between the dual modes is less than 3 dB normally, while the average power of the two working points differs usually above 10 dB due to the narrowband character of the microring modulator.

Moreover, since the last section has concluded that it is necessary for wireless signal delivery with the consistent average power of two optical carriers, we have designed a thermally tunable ring filter with a radius of 40 μm. The transmission spectrum of the on-chip ring filter shown in Fig. 4 is a Lorentz curve. It has an FSR of 282 GHz, an extinction ratio of

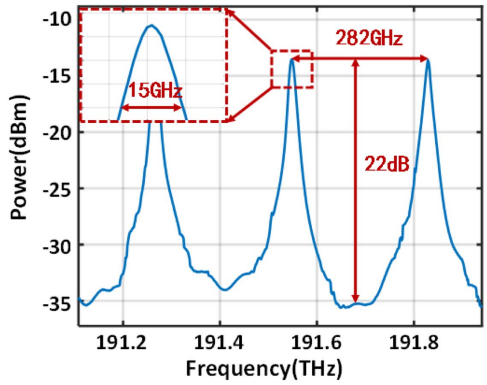

Fig. 4. Optical transmission spectrum of the on-chip ring resonator.

22 dB, and a full width at half-maximum of 15 GHz. It can not only be used as a filter to suppress other sidebands and noises but can also operate as an adjustable attenuator to adjust the output power of two modulated optical carriers. By adjusting the voltage on the electrode of the ring filter, the resonant working point can be changed. Due to the fixed frequency of the dual-mode integrated laser, the average power of two optical carriers can be adjusted by using the on-chip ring filters.

The frequency of the dual-mode DFB laser is set at 191.472 THz (−2 dBm) and 191.558 THz (−2 dBm), respectively. The required wavelength depends on the loss transmission spectral line of the microring modulators, and the optical heterodyne frequency is around 86 GHz. The optical source at 191.472 THz is modulated by the microring modulator with 10 Gb/s non-return-to-zero (NRZ) electrical signaling.

In the experiment, we compared the transmission performance of different optical sources. In addition to the integrated DFB laser, we utilize two free-running CW lasers: one (Agilent 8164A) for data transfer, and the other (PPCL550) operated as the reference light source. Figure 5(a) shows modulated eye diagram of 10 Gb/s signal without wireless transmission. Figure 5(b) shows the BER of the integrated DFB laser and the two off-chip free-running lasers, respectively. It can be seen that the use of the dual-mode DFB laser has the same reliability as that of the two free-running lasers.

C. Experiments of Introducing Cascaded Microring Modulators

The significance of dual-carrier modulation for system signal-to-noise ratio has been proved in Section 2. Compared with the single-carrier modulation, we operate the two cascaded microrings both working at optimal modulating wavelength, which means that the condition of maximum power of the wireless signal can also be realized. Therefore, the method based on modulation consistency cascaded microrings not only enables the system to obtain the higher power of the wireless signal, but also makes it easier to adjust the relative power of the two optical carriers; since compared with adjusting the working points of the two microrings, it is relatively complicated to obtain the similar average power of the two carriers with the on-chip ring filters.

By adjusting the voltage corresponding to the heater loaded on the microring modulator, we tune the wavelength corresponding to the dual-mode state of the DFB laser to match the best working point of the cascaded modulators. Figure 6 shows the transmission waveforms of two cascaded microring modulators under different reverse DC voltages from 0 V to 6 V. Figure 2(c) shows the photo of cascaded microrings and GSGSG probes. The probes of GS and SG are used for the two modulators respectively. The amplified signal is then divided into two channels through a 50:50 power divider and loaded to two microring modulators at the same time. Since the corresponding modulation directions of the two cascaded microring modulation working points and the probe directions are both opposite, the final modulated optical signals have the same phase. As shown in Fig. 6, the frequencies of the two optical carriers are 191.472 THz and 191.558 THz, respectively. The orange line in Fig. 7(a) represents the spectrum of the two optical carriers after modulation. Figure 7(b) shows the waveform comparison of single and dual modulation before wireless delivery. The two lines are the results of the BER using single modulation and dual-channel modulation, respectively in Fig. 7(c). We can see that the transmission system based on the cascaded microring modulation consistency has higher reliability under the same average power of the two optical carriers. Figures 7(d)–7(f) describe the eye diagrams without processing. Figures 7(g)–7(i) show the eye diagrams after equalization by the linear FFE equalizer with 40 tap coefficients. Under the same input power of 11.1 mW, the eye

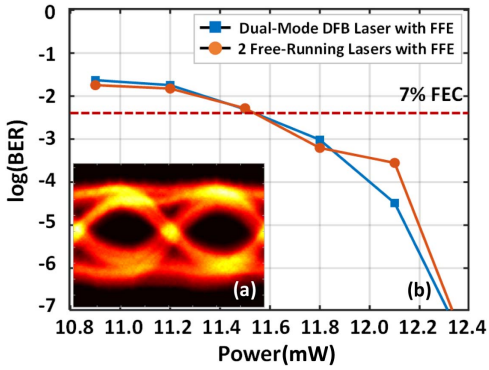

Fig. 5. (a) Eye diagram before wireless transmission. (b) BER of using different optical sources versus input optical power.

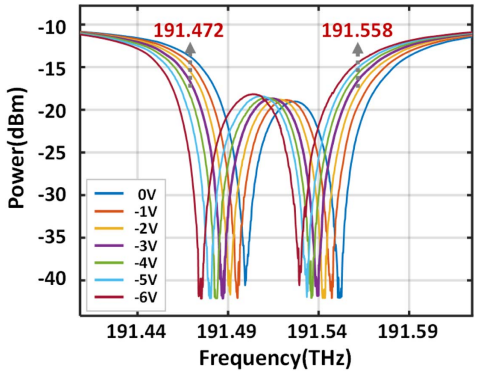

Fig. 6. Transmission spectrum of cascaded microring modulators at different voltages.

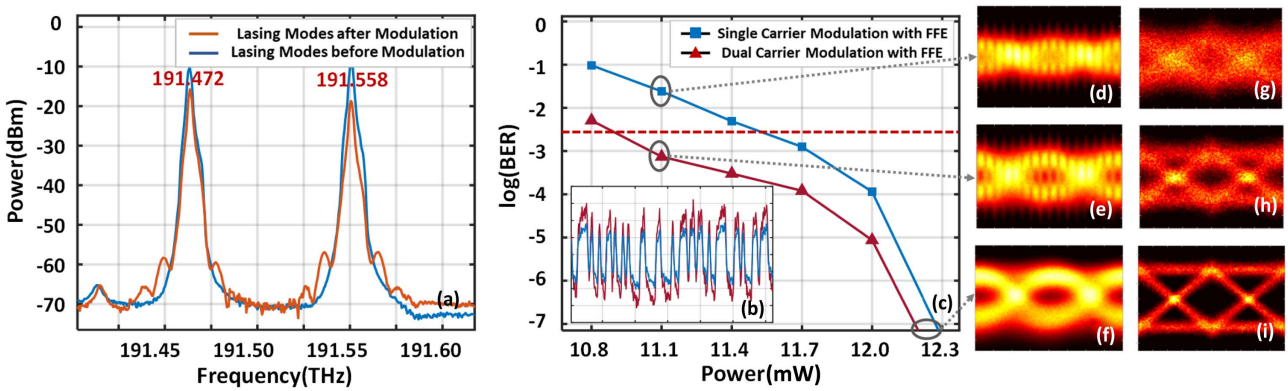

Fig. 7. (a) Spectrum of two lasing modes before and after modulation. (b) Waveform comparison without wireless transmission. (c) BER versus input optical power. (d)–(f) Eye diagrams without processing. (g)–(i) Eye diagrams with FFE equalizing.

diagram of cascaded microring modulators is clearer. The bit error rate has been reduced by over 90%. An error-free transmission is realized when the input optical power exceeds 12.3 mW.

D. Discussion

This work proves the matching degree between cascaded microring modulators and the integrated DFB laser. Moreover, the W-band transmitter shown in this paper has higher integration and lower power consumption, which can be further expanded in the future. The wavelength-division multiplexing system with an integrated DFB laser and integrated modulator was proposed in Ref. [14], but the experiment was only based on the integrated DFB laser and discrete MZM. Noting that the microring modulator is more suitable for wavelength-division multiplexing applications because of its narrowband frequency selection capability and lower footprint, multiple modulation signals can be loaded by paralleling or cascading multiple microring modulators on a chip to achieve high-capacity communication.

In addition, the loss of this integrated transmitter mainly includes the coupling loss, the modulation insertion loss, and on-chip propagation loss. The transmission loss of the waveguide is around 1.36 dB/cm according to the process design kit (PDK) from Interuniversity Microelectronics Centre (IMEC). Due to the fact that the waveguides are short in this system, the transmission loss of the waveguide can be ignored compared with other losses. As is shown in Fig. 1, the modulation insertion loss of one single microring modulator is about 8 dB. Since the transmission loss of the waveguide is ignored, the total loss of the transmitter based on the cascaded microring modulators and chip-based laser is about 22 dB. The transmission distance of this system is mainly related to the average power of millimeter wave. In this experiment, when the erbium-doped fiber amplifier (EDFA) compensates for the optical losses, the input optical power of the high-speed detector reaches the upper limit. The main reason for the limited communication distance of the system is the lack of W-band RF amplifiers.

Moreover, the transmission data rate of the system can be further improved by improving the modulation format. The bandwidth limitation of this system is mainly due to the 10 GHz bandwidth of the envelope detector. However, it has been proved in Ref. [20] that the system using higher modulation formats will be affected by signal-signal beat interference. Therefore, the modulation upper limit of this system can be further studied experimentally.

4. CONCLUSION

In this paper, the integrated dual-mode DFB laser is used as the millimeter wave source of the W-band. The single-carrier transmission of 86 GHz carrier frequency is completed based on the single-channel microring modulator. The transmission performances of the integrated DFB laser and two free-running lasers are compared experimentally. In the direct detection system, they have almost the same reliability. Aiming at the problem that the modulation depth of the microring modulator is not enough, since the dual-carrier modulation cannot be carried out due to the narrowband characteristics, this paper proposes a dual-carrier modulation scheme with cascaded microring modulation consistency, which can improve the system signal-to-noise ratio by 3 dB. The transmission performances of the single-carrier and dual-carrier modulation systems based on the microring modulator are verified by experiments. The latter has a lower signal-to-noise ratio and clearer eye diagram. The bit error rate has been reduced by over 90%. In addition, compared with the single-carrier modulation, the modulation method of transmitters using cascaded microring modulators can be well controlled.

Funding. National Key Research and Development Program of China (2019YFB1802903); National Natural Science Foundation of China (62175146, 62235011).

Disclosures. The authors declare no conflicts of interest.

Data Availability. Data underlying the results presented in this paper are not publicly available at this time but may be obtained from the authors upon reasonable request.

REFERENCES

1. S. Cherry, "Edholm's law of bandwidth," IEEE Spectr. **41**, 58–60 (2004).

2. H. Elayan, O. Amin, B. Shihada, R. M. Shubair, and M.-S. Alouini, "Terahertz band: the last piece of RF spectrum puzzle for communication systems," IEEE Open J. Commun. Soc. **1**, 1–32 (2020).
3. T. Nagatsuma, G. Ducournau, and C. Renaud, "Advances in terahertz communications accelerated by photonics," Nat. Photonics **10**, 371–379 (2016).
4. X. Li, J. Yu, and G.-K. Chang, "Photonics-aided millimeter-wave technologies for extreme mobile broadband communications in 5G," J. Lightwave Technol. **38**, 366–378 (2020).
5. D. Wake, C. R. Lima, and P. A. Davies, "Transmission of 60-GHz signals over 100 km of optical fiber using a dual-mode semiconductor laser source," IEEE Photonics Technol. Lett. **8**, 578–580 (1996).
6. A. Nirmalathas, H. F. Liu, Z. Ahmed, D. Novak, and Y. Ogawa, "Subharmonic synchronous and hybrid mode-locking of a monolithic DBR laser operating at millimeter-wave frequencies," IEEE Photonics Technol. Lett. **9**, 434–436 (1997).
7. J. Yu, Z. Jia, T. Wang, and G. K. Chang, "Centralized lightwave radio-over-fiber system with photonic frequency quadrupling for high-frequency millimeter-wave generation," IEEE Photonics Technol. Lett. **19**, 1499–1501 (2007).
8. R. Puerta, J. Yu, X. Li, Y. Xu, J. J. V. Olmos, and I. T. Monroy, "Single-carrier dual-polarization 328-Gb/s wireless transmission in a D-band millimeter wave 2 × 2 MU-MIMO radio-over-fiber system," J. Lightwave Technol. **36**, 587–593 (2018).
9. J. Xie, W. Ye, L. Zhou, X. Guo, X. Zang, L. Chen, and Y. Zhu, "A review on terahertz technologies accelerated by silicon photonics," Nanomaterials **11**, 1646 (2021).
10. G. Carpintero, S. Hisatake, D. de Felipe, R. Guzman, T. Nagatsuma, and N. Keil, "Wireless data transmission at terahertz carrier waves generated from a hybrid InP-polymer dual tunable DBR laser photonic integrated circuit," Sci. Rep. **8**, 3018 (2018).
11. Y. Liu, B. Isaac, J. Kalkavage, E. Adles, T. Clark, and J. Klamkin, "93-GHz signal beam steering with true time delayed integrated optical beamforming network," in *Optical Fiber Communication Conference (OFC)* (Optica, 2019), paper Th1C.5.
12. S.-R. Moon, S. Han, S. Yoo, H. Park, W.-K. Lee, J. K. Lee, J. Park, K. Yu, S.-H. Cho, and J. Kim, "Demonstration of photonics-aided terahertz wireless transmission system with using silicon photonics circuit," Opt. Express **28**, 23397–23408 (2020).
13. M. Che, Y. Matsuo, H. Kanaya, H. Ito, T. Ishibashi, and K. Kato, "Optoelectronic THz-wave beam steering by arrayed photomixers with integrated antennas," IEEE Photonics Technol. Lett. **32**, 979–982 (2020).
14. S. Jia, M. C. Lo, L. Zhang, O. Ozolins, A. Udalcovs, D. Kong, X. Pang, R. Guzman, X. Yu, S. Xiao, S. Popov, J. Chen, G. Carpintero, T. Morioka, H. Hu, and L. K. Oxenløwe, "Integrated dual-laser photonic chip for high-purity carrier generation enabling ultrafast terahertz wireless communications," Nat. Commun. **13**, 1388 (2022).
15. E. Lacombe, C. Belem-Goncalves, C. Luxey, F. Gianesello, C. Durand, D. Gloria, and G. Ducournau, "10-Gb/s indoor THz communications using industrial Si photonics technology," IEEE Microw. Wireless Compon. Lett. **28**, 362–364 (2018).
16. N. Shimizu and T. Nagatsuma, "Photodiode-integrated microstrip antenna array for subterahertz radiation," IEEE Photonics Technol. Lett. **18**, 743–745 (2006).
17. Y. Xu, J. Lin, R. Dubé-Demers, S. LaRochelle, L. Rusch, and W. Shi, "Integrated flexible-grid WDM transmitter using an optical frequency comb in microring modulators," Opt. Lett. **43**, 1554–1557 (2018).
18. S. Jia, M. Lo, D. Kong, R. Guzman, L. Li, L. K. Oxenløwe, G. Carpintero, and H. Hu, "Integrated dual-DFB laser chip-based PAM-4 photonic-wireless transmission in W-band," in *Optical Fiber Communication Conference (OFC)* (Optica, 2021), paper F4F.3.
19. K. Balakier, M. J. Fice, F. van Dijk, G. Kervella, G. Carpintero, A. J. Seeds, and C. C. Renaud, "Optical injection locking of monolithically integrated photonic source for generation of high purity signals above 100 GHz," Opt. Express **22**, 29404–29412 (2014).
20. L. Gonzalez-Guerrero, M. Ali, R. Guzman, H. Lamela, and G. Carpintero, "Photonic sub-terahertz IM links: comparison between double and single carrier modulation," J. Lightwave Technol. **40**, 6064–6070 (2022).